**ARI** The Bulletin of the Istanbul Technical University VOLUME 53, NUMBER 1
Communicated by Ali Göktan

# Experimental and Numerical Study in Evaporation of Hydrocarbon Droplet Surface Temperature

Mohamed Bouaziz, Joseph Dgheim, Martine Grisenti, Jacky Bresson, and Belkacem Zeghmati
*C.E.F.G.M.A.I., UPRES EA 2986, Université de Perpignan*
*52, Avenue de Villeneuve, 66860 Perpignan Cedex France*
(Received 12 July 2002)

Time evolution of droplet radius regression and surface temperature are studied experimentally and numerically by evaporating a single droplet of pure fuel or fuel mixture in either hot air flow or natural convection. The droplet was suspended on a capillary setup inside the test section of a thermal wind-tunnel. A video system and an infrared camera recorded video and thermal images during droplet evaporation sequences. The model of the "film theory" based on conservation equations is used and experiments are compared to calculations for several heptane-decane or octane-hexane mixtures and for pure products. The experimental data are in good agreement with the calculated results.

**Keywords:** Evaporation, surface temperature, heat transfer, mass transfer, fuel mixture.

## 1. Introduction

Radius regression and surface temperature of an evaporating droplet has been the subject of many numerical and experimental studies [1, 6] because of their interest in many technical systems. A study where the technique used is a droplet hung to a thermocouple is presented by Downing [7], who carried out tests with various thermocouple diameters to extrapolate data and to obtain results corresponding to a zero value of thermocouple diameter. Roth et al. [8] used the optical technology of "rainbow" refractometry based on the relationship between the refraction factor of the liquid and its temperature. Nana et al. [9] and Naudin [10] realized and implemented a system of measurement, based on infrared thermography, which follows the evolution of surface temperature of an evaporating methanol droplet.
Surface temperature measurement by using a non-intrusive technique such as infrared thermal imaging, necessarily implies the knowledge of its emissivity. The determination of the emissivity of the opaque and semi-transparent mediums such as liquids and gases raises many unsolved problems.
The emissivity and the surface temperature of small droplets (diameters equal to a few microns) of ethanol and methanol liquids is determined by Nana [9] and Naudin [10] by using an infrared detector, the Mie theory and the Kirschoff law.
Water droplet diameters varying between 0.01 and 20 $\mu$m have an emissivity determined by Pluchino [11] by using the Maxwell equations (Mie theory) and the Kirchhoff law. He found an emissivity higher than 1, which is in contradiction with the definition of the emissivity.
This work follows a numerical model and measurements of droplet radius evolution in evaporation, already studied in our laboratory by Daïf et al [12, 13]. The model is based on the film concept and provides time evolution of the radius and surface temperature of a pure or mixed liquid droplet in evaporation in natural or forced convection. The originality of the present paper is the use of an infrared camera for the determination of droplet surface temperature from thermal images. The method shows that temperature is a more sensitive parameter than the droplet radius regression.
Experimentally, the liquid droplet is suspended at the center of the thermal test section at the extremity of a glass capillary. Optical access is provided on each side of the test section to observe and record the evolution of both the droplet diameter followed by a camcorder and the surface temperature by means of an infrared camera. Finally, the numerical results are compared to the experimental ones for pure and mixed liquid droplets.

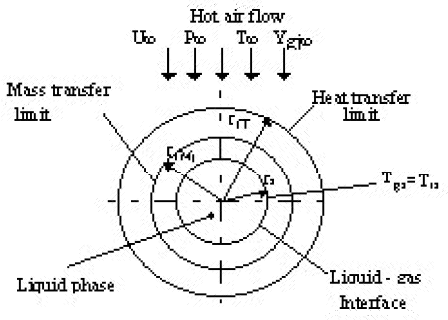


Figure 1. Physical model of the droplet vaporization in a gaseous film.

## 2. Numerical model

Our model [12, 13] is a generalization of the model proposed by Abramzon and Sirignano [14], extended to the vaporization of a mixed droplet in forced convection [11] and a pure or binary fuel droplet in natural convection [12]. This model is based on the film theory, where mass and heat transfers between the droplet surface and the external gas are considered to take place inside a thin gaseous film surrounding the droplet (fig.1). At any time the thickness of the film depends on the average Nusselt and Sherwood numbers that qualify these transfers. Film thickness limits the integration areas of the mass and energy conservation equations in the gaseous phase.

Transfer equations are discretized by using an implicit finite difference method. For each equation, the discretization leads to algebraic equation system, which is solved by Thomas algorithm. The system solution determines the temperature distribution inside the droplet. In the case of the mixture and in addition to energy equation in the liquid phase, mass distribution equations are solved to determine the spatial evolution of the mass fraction.

$$\frac{\partial T_l}{\partial t} = \frac{\overline{\alpha}_l}{r^2}\frac{\partial}{\partial r}(r^2\frac{\partial T_l}{\partial r}) \tag{1}$$

$$\frac{\partial Y_{lj}}{\partial t} = \frac{\overline{D}_{lj}}{r^2}\frac{\partial}{\partial r}(r^2\frac{\partial Y_{lj}}{\partial r}) \tag{2}$$

Mass and thermal balance are constantly verified at the surface of the droplet. The external radius limiting the integration areas of the conservation equation in the gaseous phase is defined by Abramzson and Sirignano [14] and depends on the modified Nusselt and Sherwood numbers:

$$r_{fT} = \frac{r_s\overline{Nu}^*}{\overline{Nu}^* - 2} \tag{3}$$

$$r_{fMj} = \frac{r_s\overline{Sh_j}^*}{\overline{Sh_j}^* - 2} \tag{4}$$

where $\overline{Nu}^*$ and $\overline{Sh_j}^*$ represent modified average Nusselt and Sherwood numbers [14].
The correlations defining the average Nusselt and Sherwood numbers in natural convection are essentially a function of Grashof numbers. They are proposed by authors [12, 15] for a hydrocarbon or hydrocarbon mixture:

$$\overline{Nu} = 2 + 0.591(1+B_T)^{-0.588}Pr^{\frac{1}{3}}Gr_m^{\frac{1}{4}} \tag{5}$$

$$\overline{Sh_j} = 2 + 0.574(1+B_M)^{-0.089}Sc_j^{\frac{1}{3}}Gr_m^{\frac{1}{4}} \tag{6}$$

With :

$$10^{-3} \leq Gr_m \leq 8.10^4$$
$$0 \leq B_T \leq 2.6$$
$$0 \leq B_M \leq 2.44$$

In forced convection, the correlations which are a function of Reynolds number, are proposed by Renksizbulut et al. [16] :

$$\overline{Nu} = (2 + 0.57Re_m^{\frac{1}{2}}Pr^{\frac{1}{3}})(1+B_T)^{-0.7} \tag{7}$$

$$\overline{Sh_j} = (2 + 0.87Re_m^{\frac{1}{2}}Sc_j^{\frac{1}{3}})(1+B_T)^{-0.7} \tag{8}$$

with : $10 \leq Re_m \leq 300$
Correlations (5, 6) and (7, 8) describing phenomena respectively in natural and forced convection, are equivalent and equal to 2 when $Gr_m$ and $Re_m$ tend to zero. Thermal numbers $B_T$ and mass transfer number $B_M$ also tend to zero.
Relations between $\overline{Nu}^*$, $\overline{Sh_j}^*$ and $\overline{Nu}$, $\overline{Sh_j}$ are given by Abramzson and Sirignano [14] :

$$\overline{Nu} = \overline{Nu}^*\frac{\ln(1+B_T)}{B_T} \tag{9}$$

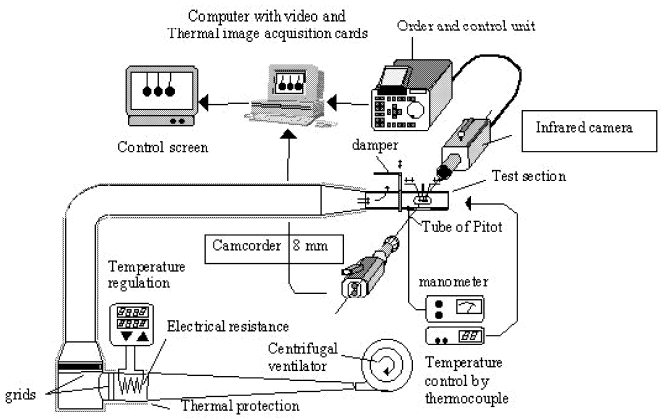


Figure 2. Wind tunnel and measuring instruments.

$$\overline{Sh_j} = \overline{Sh_j}^* \frac{\ln(1+B_M)}{B_M} \tag{10}$$

The model allows to determine surface temperature, radius regression and mass fraction.

## 3. Experimental setup and computer image processing

The experimental setup (fig. 2) is used to evaporate pure or mixed liquid droplet at atmospheric pressure by recording video and thermal images. The synchronization of thermal recordings and video images is time based simultaneously.

### 3.1. The thermal wind-tunnel

The setup includes a rectangular test section situated at the horizontal end of a thermal wind-tunnel. Air flow in the experimental channel is homogenized by grids. A thermal protection insulates the hot part of the wind-tunnel and limits heat losses. In the test section, hot air flow, the average velocity of which varies between 0 and 10 m.s$^{-1}$, is generated by a centrifugal fan. The flow is heated by means of two heating elements placed inside the experimental setup. Temperature is controled by a regulator, which maintains a maximum constant temperature of 423 K in the test section.

The pure or mixed liquid droplet is hung at the center of the test section at the extremity of a glass capillary (diameter 0.2 to 0.3 mm) fixed on a permanent holder. In the case of mixed liquid, those are prepared and sampled by a hypodermic syringe constantly shaken to maintain the mixture homogeneity. When the droplet leaves the injection needle, one considers that the droplet is made up of a homogeneous product corresponding to the prepared mixture. The phenomenon can be observed optically on each side of the test section. The recording begins just before the droplet is suspended. This apparatus is provided with a mechanical device situated at the entrance of the measurement test section:

- when it is closed, hot air flow is ejected from the device without passing through the test section, which keeps velocity and temperature at permanent regime inside the other parts of the experimental setup. The droplet is introduced on the holder with a syringe in the test section at the room temperature.
- when it is opened, the heated flow enters the test section, and the sequence of measurement in forced convection can begin. The air temperature is measured by a thermocouple and the velocity is controlled by a Pitot tube connected to a manometer.

For tests in natural convection, the damper and the exit of the test section are closed.

### 3.2. Infrared system and thermal image processing

The infrared thermography system is composed of an infrared camera (Inframetrics Models 760, 3-12 $\mu$m) equipped with two lenses: a telescope (3X) and a close-up lens, and with an order and control unit for thermal sequence recording. A video camcorder completes the system. Recorded thermal sequences are processed after acquisition by a specialized software (Thermagram), which determines the surface temperature evolution during evaporation.

### 3.3. Video system and image processing

Sequences of evaporation are also recorded by a video system (camcorder 8 mm - charge coupled device, 470000 pixels) equipped for macrophotography. A processing computer (image acquisition board and software) digitalizes and compresses video sequences with a maximum speed equal to 25 images/s. The spatial definition of an image after decompression is 320x240 pixels. The

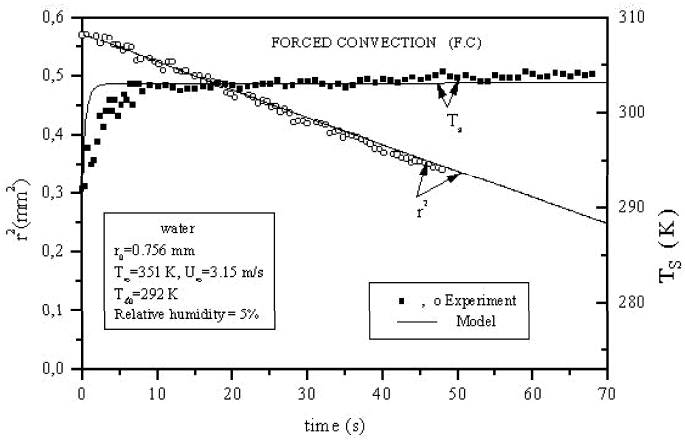


Figure 3. Time evolution of the surface temperature and square radius of a water droplet evaporated in a hot air flow.

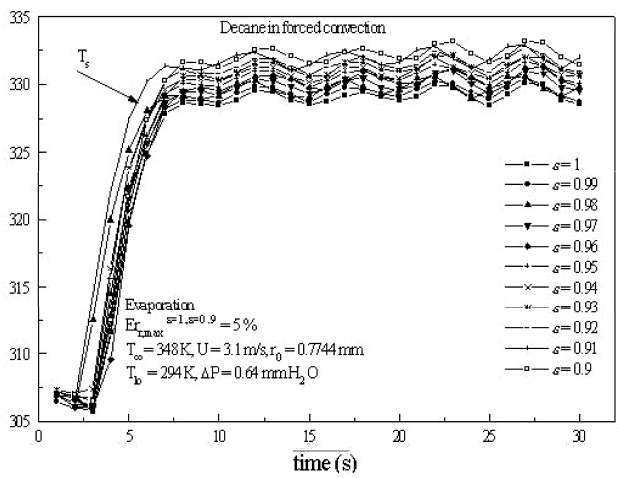


Figure 4. Time evolution of the surface temperature for various emissivities of a decane droplet evaporated in forced convection.

droplet in evaporation is illuminated from the rear of a luminous base, which increases the contrast and facilitates the extraction of the droplet outlines. The droplet appears opaque on the control screen and the base rather white. Digital images present a high contrast in grays between the droplet and the base. This facilitates the extraction of the droplet contour, which is obtained by scanning and detecting the gray level of the pixels of each image line. The droplet is assumed to have symmetry of revolution from which the real volume of the droplet is deduced. The equivalent radius of a sphere of the same volume is then determined to initialize the numerical model and to obtain the radius regression related to the time.

## 4. Results and discussion

Experimental and numerical results of the evaporation of pure liquid droplets (water, decane, octane, heptane and hexane) and mixed liquid droplets (octane-hexane and heptane-decane) of different initial compositions are presented. The droplet diameter varied between 1.1 and 1.55 mm. Temperature profiles obtained by an infrared camera are compared to the ones of the numerical results.

### 4.1. Evaporation of a pure hydrocarbon droplet

Water droplet evaporation of known emissivity [17] ( $\epsilon = 0.96$) is studied to observe the validity of the theoretical model and the experimental results. Figure 3 indicates the evaporation of a water droplet in forced convection. It seems that the numerical model is in good agreement with the experimental results for the surface temperature as well as for the radius regression.

In general, liquid hydrocarbons average emissivity lies between 0.9 and 1 [17, 19]. Figure 4 shows the evolution of decane liquid droplet surface temperature measured by an infrared camera of thermal imaging, for various average emissivity values ($\varepsilon = 0.9$ to 1). So, if the measured temperature for a mean emissivity is equal to 1 as a reference temperature, the relative error is equal to 5 % for a measured temperature with a mean emissivity equal to 0.9. Thus, we conclude a good agreement between both experimental and numerical results. In fact, our theoretical results lead to a temperature distribution very close to that obtained experimentally by an emissivity of 0.95 (fig.5). It is very clear that the numerical model is in good agreement with the experimental results for the surface temperature as well as for the radius regression (error inferior to 5 %). In the following, our experimental results are obtained for an av-

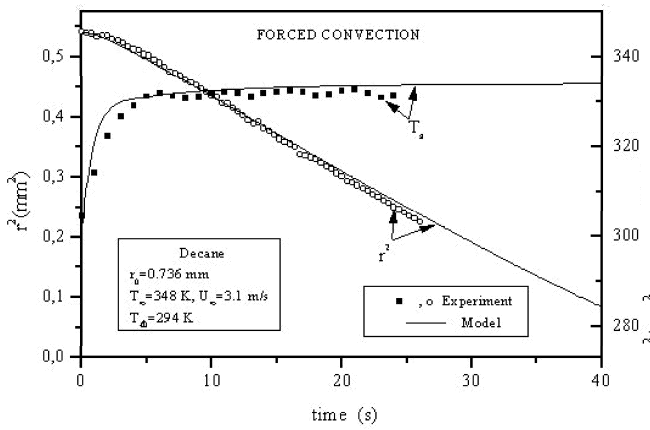


Figure 5. Time evolution of the surface temperature and square radius of a decane droplet evaporated in a hot air flow.

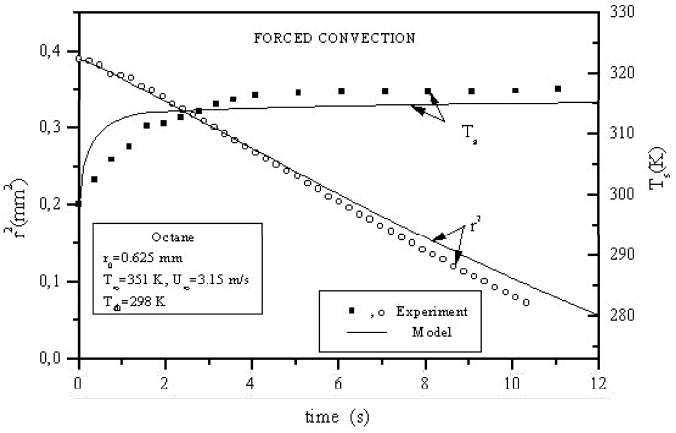


Figure 6. Time evolution of the surface temperature and square radius of a octane droplet evaporated in a hot air flow.

erage emissivity equal to 0.95.

Results of the evaporation of an octane droplet in forced convection (fig.6), heptane (fig.7) and hexane (fig.8) in natural convection, show globally a good agreement between experimental and numerical results. The little disagreement at the beginning of the evaporation (fig. 4 through 8) originates in simplifying hypothesis assumed to set the model that does not correctly take into account the internal circulations in the droplet and the heat transfer between the droplet and the capillary. The experimental conditions in forced and natural convections are differents. In fact, the experimental set up is not appropriate to regulate the air temperature and velocity around the liquid droplet. So, the comparison between natural convection evaporation and forced convection evaporation for the same liquid droplet is impossible.

### 4.2. Evaporation of mixture hydrocarbon droplet

Figures 9, 10 and 11 show time evolution of the square radius regression and the surface temperature of mixture droplet (octane-hexane) in evaporation in natural convection, three initial compositions are studied. The evaporation decomposes in two stages :

- A cooling stage, all the more pronounced (minimum temperature) that the mixture contains more hexane (the more volatile

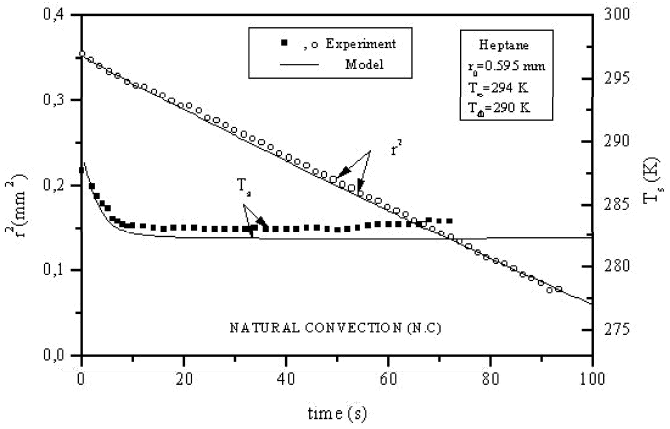


Figure 7. Time evolution of the surface temperature and square radius of a heptane droplet evaporated in natural convection.

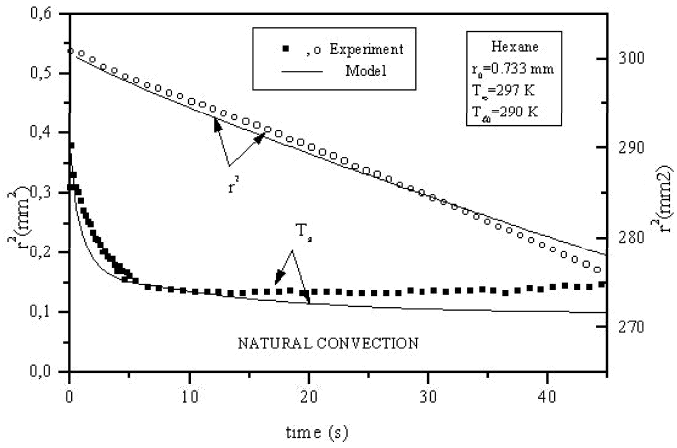


Figure 8. Time evolution of the surface temperature and square radius of a hexane droplet evaporated in natural convection.

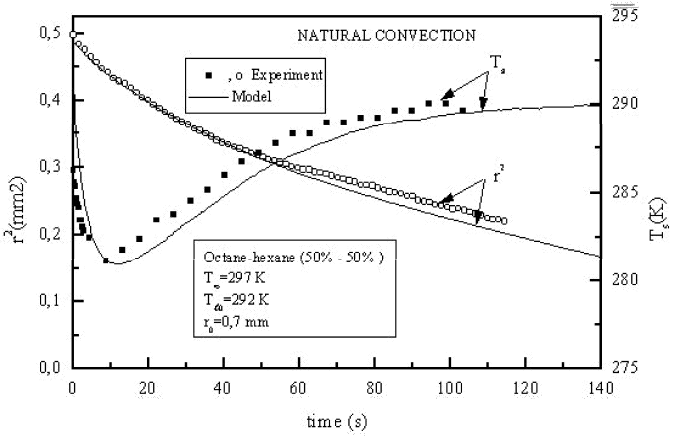


Figure 10. Time evolution of the surface temperature and square radius of a mixture droplet (initial composition): (50% of octane and 50% of hexane) evaporated in natural convection.

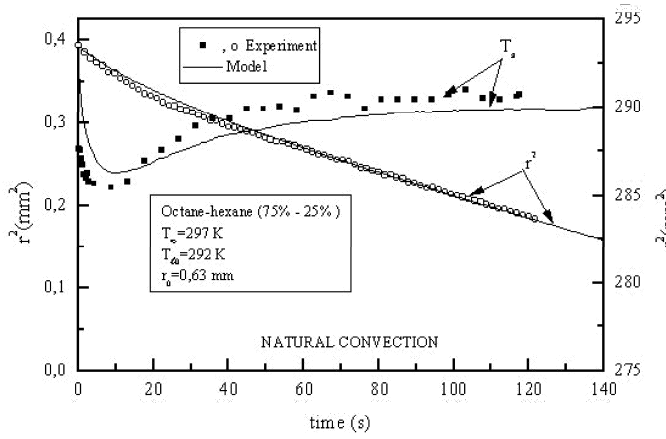


Figure 9. Time evolution of the surface temperature and square radius of a mixture droplet (initial composition) : (75% of octane and 25% of hexane) evaporated in natural convection.

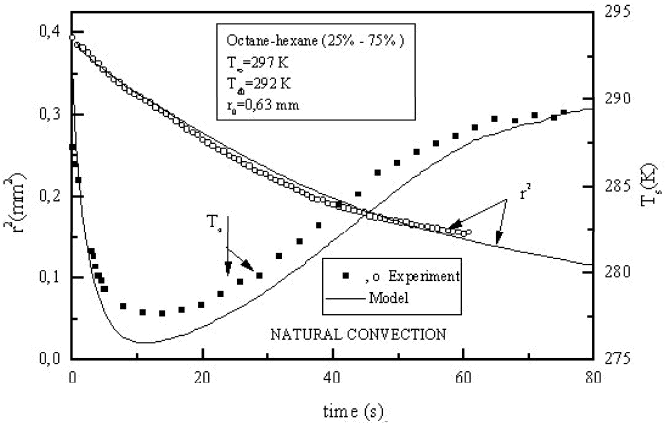


Figure 11. Time evolution of the surface temperature and square radius of a mixture droplet (initial composition): (25% of octane and 75% of hexane) evaporated in natural convection.

component)

- A warming stage until the humid vapor temperature of the octane (the less volatile component) whatever the initial composition of the mixture is considered.

This phenomenon shows the existence of a sequential evaporation. The error between the experimental and the theoretical curves is less than 10 %. So, we can conclude that our numerical results are in good agreement with the experimental ones for the droplet with single component as well as the droplet with multi components in natural convection.
The vaporization in forced convection of mixed liquid droplet (heptane-decane) is also studied for three initial compositions (fig. 12, 13 and 14). These experiments took place during two periods :

- the first one in natural convection (N.C), during the suspension of the droplet. At the outset, the droplet presents a homogeneous mixture, then as soon as the vaporization begins, the difference in the volatility of the constituent (the heptane more volatile than the decane) produces an evolution of the droplet composition. The mass fraction of each component varies from the center to the surface of the droplet. This evolution is correctly anticipated by our model in natural convection by means of equation (2) resolution,

- the second one in forced convection (F.C), when the hot air flow penetrated the test section. The model in natural convection is used to determine these conditions (radius, temperature and particularly mixture composition) and to initialize the model in forced convection. The comparison between models and experimental results seems satisfactory. As on previous curves, the sequential evaporation phenomenon is visible, particularly on figure 14, which shows, at the beginning of the forced convection, the influence of the more volatile component (heptane) that makes the temperature tends to an asymptotic value corresponding to its saturating vapor temperature. At the end of the evaporation, the curve tends to the saturation temperature of the remaining component (decane). Such phenomenon

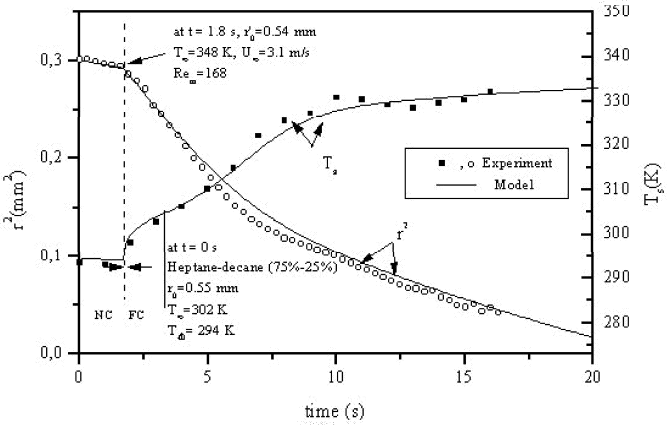


Figure 12. Time evolution of the surface temperature and square radius of a mixture droplet (initial composition): (75% of heptane and 25% of decane) evaporated in natural convection.

also appeared on the curves of the radius regression versus time, for which a slope change characterized the sequential vaporization.

## 5. Conclusion

This work presents a numerical and experimental study of radius regression and surface temperature evolution of a pure or mixed liquid droplet in evaporation. Vaporization took place in natural or forced convection. Experiments used an infrared camera to determine the surface temperature of the droplet and a camcorder to follow simultaneously the droplet diameter evolution. The numerical model based on the film concept, assumes that the droplet is surrounded by gaseous films, in which mass and thermal transfer take place.
A preliminary study on the evaporation of a single droplet in forced and natural convection shows a good agreement between the model and the experiment for the surface temperature and the square radius regression.
- In natural convection, droplet surface temperature decreases until it reaches vapor phase saturation temperature because the evaporation is accompained by a reduction in droplet heating,
- In forced convection, droplet surface temperature increases from liquid droplet temperature to

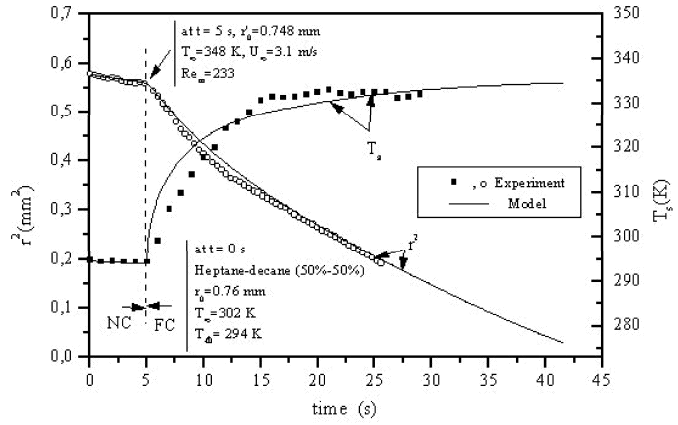


Figure 13. Time evolution of the surface temperature and square radius of a mixture droplet (initial composition): (50% of heptane and 50% of decane) evaporated in natural convection.

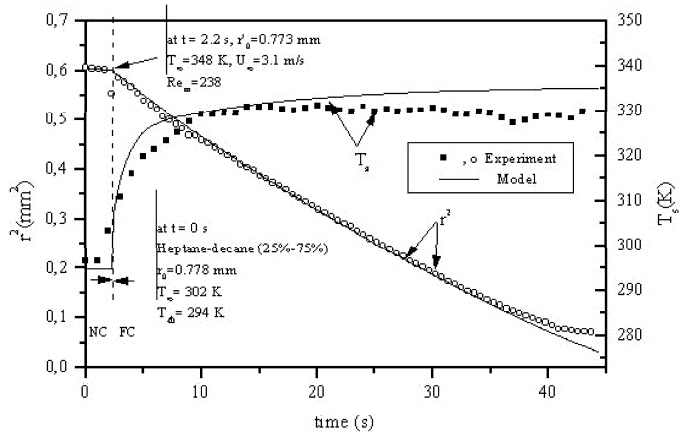


Figure 14. Time evolution of the surface temperature and square radius of a mixture droplet (initial composition : (25% of heptane and 75% of decane) evaporated in natural convection.

its saturation value because the ambient medium temperature is superior to that of the liquid droplet.

Droplet square radius decreases with time evolution and verifies the $d^2$ law.

A later study is realized for the bicomponents evaporating in natural and forced convection. This study shows that the evaporation of bicomponent liquid droplets has the same qualitative evolution as that of the monocomponent but it is influenced by the initial compositions of the fuel droplets. Droplet evaporation curves show the difference stages of the evaporation phenomena and indicate that the experimental data are in good agreement with the numerical results for radius regression and for the surface temperature evolution.

## 6. Nomenclature

$B_M$ : mass transfer number
$B_T$ : heat transfer number
$Cp$ : specific heat at constant pressure J.kg$^{-1}$.K$^{-1}$
$D$ : diffusion coefficient m$^2$.s$^{-1}$
$g$ : gravitational constant m.s$^{-2}$
$Gr_T$ : thermal Grashof number
$Gr_{Mj}$ : mass Grashof number of the j component
$Gr_m$ : average Grashof number
$M$ : molecular weight kg
$Nu$ : Nusselt number
$Pr$ : Prandtl number
$q_g$: heat transferred into the droplet J.kg$^{-1}$
$r$ : droplet radius m
$r_{fM}$ : limit of the integration area for mass transfer
$r_{fT}$ : limit of the integration area for heat transfer
$Re_m$ : average Reynolds number
$Sc$ : Schmidt number
$Sh$ : Sherwood number
$t$ : time s
$T$ : temperature K
$U$ : air velocity m.s$^{-1}$
$Y$ : mass fraction

**Greek letters**

$\beta_T$: thermal expansion coefficient of the fluid
$\beta_{Mj}$: mass expansion coefficient of the j component
$\mu$: dynamic viscosity kg.m$^{-1}$.s$^{-1}$
$\lambda$: kinematic viscosity m$^2$.s$^{-1}$
$\rho$: density kg.m$^{-3}$

**Subscripts**
$f$ : film
$g$ : gas
$j$ : component index j=1, 2
$l$ : liquid
$T$ : thermal
$M$ : mass
0 : initial
$s$ : surface
$\infty$ : ambient gas
**Superscripts**
$*$ : modified number

## References


[1] M. Mawid and S. K. Aggarwal, Combust. and Flame **84** , 197 (1991).
[2] C. K. Law, T. Y. Xiong, and C. H. Wang, Int. J. Heat Mass Transfer **30**, 1435 (1987).
[3] D. G. Talley and S. C. Yao, A semi empirical approach to thermal and composition transients inside vaporising fuel droplets, The Combustion Institute, 609 (1986).
[4] C. K. Law, Prog. Energy Combust. Sci. **8**, 171 (1982).
[5] G. Continillo and W. A. Sirignano, Numerical study of multicomponent fuel spray flame propagation in a spherical closed volume, 22em Symposium (international) on Combustion, The Combustion Institute, Pittsburgh, PA, 1941 (1988).
[6] C. Chauveau, X. Chesneau, and I. Gökalp, "High pressure vaporization and burning of methanol droplets in reduced gravity", AIAA Congress 940 (1994).
[7] C. G. Downing, Ph.D. thesis, University of Wisconsin, Madison (1960).
[8] N. Roth, K. Anders, and A. Frohn, J. Laser Applications 37 (1990).
[9] L. Nana, J. Farre, and A. Giovannini, Revue pratique de contrôle industriel **31**, 60 (1992).
[10] N. Naudin, Thesis, ENAC (1995).
[11] A. B. Pluchino, Applied Optics **18**, 4065 (1979).
[12] A. Daïf, A. Ali Chèrif, J. Bresson, and B. Sarh, Journal de Physique III **5**, 1643 (1995).
[13] A. Daïf, M. Bouaziz, and M. Grisenti, J. Therm. Heat Transfer **12**, 107 (1998).
[14] B. Abramzson and W. A. Sirignano, International Journal of Heat and Mass Transfer **32**, 1605 (1989).
[15] M. Bouaziz, A. Daïf, A. Ali Chèrif, and X. Chesneau, "Numerical Determination of the Correlations Qualifying the Mass and Heat Transfert Around a Sphere Saturated with a Pure Liquid in Natural Convection", Book of abstracts of Inter. Symp. on Advances in Comput. Heat Transfer, Int. Centre Heat Mass Transfer, Cesme, Turkey, 222 (1997).
[16] M. Renksizbulut, R. Nafziger, and X. Li, Chemical Engineering Science **46**, 2351 (1991).
[17] J. R. Singham, International Journal of Heat and Mass Transfer **5**, 67 (1962).
[18] M. H. Friedman and S.W. Churchill, "The absorption of thermal radiation by fuel droplets", Chemical Engin. Progress Symp., 61 (1965).
[19] L. Nana, Thesis, ENSAE (1993).